Water's behaviour on Ca-rich tricalcium silicate surfaces for various degrees of hydration A molecular dynamics investigation

J. Claverie, Fabrice Bernard, J.M.M. Cordeiro, Siham Kamali-Bernard

Water's behaviour on Ca-rich tricalcium silicate surfaces for various degrees of hydration: A Molecular Dynamics investigation

Jérôme Claverie[a,b], Fabrice Bernard[a], João Manuel Marques Cordeiro[b], Siham Kamali-Bernard[a]

[a] *Laboratory of Civil Engineering and Mechanical Engineering (LGCGM), INSA Rennes, Rennes, France*
[b] *Department of Physics and Chemistry, School of Natural Sciences and Engineering, São Paulo State University (UNESP), 15385-000 Ilha Solteira, São Paulo, Brazil*

Abstract

Tricalcium silicate (C_3S) hydration is a highly relevant topic toward a better understanding of ordinary Portland cement. Molecular Dynamics (MD) simulations can provide relevant information about water behaviour at interface with mineral surfaces. For the first time, the influence of C_3S protonation on water structure and dynamics is assessed by simulating the Ca-rich (040) surface in contact with water. The recently extended INTERFACE force field for C_3S, including parameters for hydroxyl and silanol groups, was used to perform classical MD calculations. The water layered structure arising from strong hydrogen bonding with the mineral surface decays with increasing hydration of the first atomic layer. We found that the presence of hydroxyl and silanol groups, as well as desorption of calcium cations strongly influence the structural and dynamical properties of water.

Keywords: Hydration, Tricalcium silicate C_3S, Molecular dynamics (MD) simulations, Hydrogen bonding

Email address: siham.kamali-bernard@insa-rennes.fr (Siham Kamali-Bernard)

1. Introduction

Concrete is fairly the most used material on Earth and constitutes most of the infrastructure of our society. The universal and systematic using of concrete in the construction industry is responsible for serious damage to the environment, mainly related to cement production, which contributes to approximately 8 percent of global CO_2 anthropogenic emissions [1]. The stoichiometry and structure of cement minerals can vary considerably depending on the proportions of raw materials and heat treatment. Each mineral has multiple polymorphs, whose reactivity can differ from each other. A better understanding of the structure and reactivity of these polymorphs is a key step towards a more sustainable design. The tricalcium silicate (Ca_3SiO_5, or C_3S in cement chemistry notation) is the major constituent of Portland cement. It reacts quickly with water and is the principal responsible for the strength development in the early ages of hydration. As a matter of fact, even before hydration by mixing water, the first exposed layers of C_3S undergo hydration depending on the relative humidity of the environment, responsible for a decrease in surface energy [2–5].

In recent years, many scientific contributions of atomistic simulations of calcium silicate hydrate (C-S-H) [6–14], tobermorite [15, 16], portlandite ($Ca(OH)_2$) [17–21] and clinker constituents [22–29] were carried out, giving rise to a force field database [30]. Although many studies are focused on the main hydration product (C-S-H), an insight on the early hydration of C_3S was performed both with reactive [24], and classical MD [31], and is crucial to explain the mechanisms responsible for the induction period. To our knowledge, two classical force fields; namely INTERFACE FF (IFF) [32], and ClayFF [33], and the reactive force field ReaxFF [34] were already used to simulate the interface between C_3S and water at the atomic scale. Despite its ability to capture bond breaks occurring during the hydration process such as dissociation of water, protonation of superficial anions, as well as the proton hopping phenomenon [24], the ReaxFF is limited by its computational cost and its charge equilibration

method. This method has been improved to correct unrealistic charge-transfer issues, but has not been implemented in the Ca-Si-O-H description yet [30, 35]. Although it reproduces accurately the bulk properties of a wide range of mineral systems, ClayFF parameters does not account for covalent bonding other than in hydroxyl groups. Thus, the covalent contribution of bonds in silicates are underestimated compared to the ionic contribution. In fact, the original ClayFF charge for tetrahedral silicon is 2.1e, which is a main difference with the value adopted in IFF (1.0e) [26, 30, 36]. The IFF offers consistent descriptions of chemical bonding and dipole moments, allowing to describe both bulk and surface properties accurately. The IFF for C_3S reproduced structural properties in good agreement with experimental results, and was employed to compute cleavage, agglomeration and grinding aids adsorption energy in dry or wet condition [26]. The first model, including parameters for the dry C_3S as well as superficial hydroxyl group, was extended to take into account further hydration steps, by adding parameters for silanol groups. The authors related the protonation state with the pH of the system, based on pKa values of free silicic acid in solution [31]. A more recent work, employing ClayFF, allowed to assess structural and dynamical properties of water and ions, as well as dissolution of C_3S in sodium sulfate solution [37]. A "geochemical" theory, which associates the rate of dissolution to the undersaturation of the solution with regards to C_3S could explain experimental observations such as etch-pits at the surface of cement grains [2, 38]. However, at the molecular scale, a quantitative approach of the dissolution of C_3S in water should be performed with precautions. A classical MD investigation cannot describes accurately dissociation mechanisms which are mainly related to reactive events. However, the study of water properties at the interface with the mineral could give a first insight on the understanding of the hydration reaction and its influence on the behavior of water close to the mineral surface.

At the interface with solid surfaces, the structure and dynamics of water are affected by several effects. First, superficial dipolar moments induce an electrostatic field into the fluid. Second, the excluded volume, or “hard-wall”

effect induces the packing of water molecules because of the spatial geometrical constraint created by the surface on water molecules [39]. Moreover, within a critical distance, water-surface and water-water hydrogen bonds lead to a layered water structure [39, 40], more disordered than ice nonetheless. The diffusion coefficient of water molecules in these layers is lowered, affecting local density and viscosity. To consider such a heterogeneous behaviour, MD overcomes the limitation of continuum mechanics methods by defining the fluid as discrete molecules [41].

In this paper, the structural and dynamical properties of water at the interface with monoclinic C_3S (040) surface are simulated using a classical force field. IFF is chosen for its ability to reproduce surface and interfacial properties and the recently developed parameters for hydrated C_3S are used [31]. As far as we know, the change in behaviour of water molecules at the interface with C_3S with hydration of the surface has never been assessed. In our computational scheme, various degree of hydration of the first atomic layer are considered, covering the range of pH at which cement hydration usually occurs. For each degree of hydration, interfacial energies, atomic densities, orientation of superficial water molecules and pair distribution functions analysis allow to describe the structural properties of the C_3S/water interface. Finally, diffusion coefficients and hydrogen bonds density and lifetime were computed to depict the dynamic of water molecules near the mineral surface, strongly influenced by hydrogen bonding.

2. Methods

In industrial clinker, C_3S crystallizes preferentially into monoclinic M_1 and M_3 polymorphs. The M_3 polymorph does not exist in pure C_3S and its stabilization is favoured by high MgO contents [42]. Despite this fact and as a first attempt to understand the features C_3S/water interface, the 2D periodic models used here were built from the pure M_3 crystal structure [43], which has been largely used in atomistic simulations [24, 26, 44] (see Fig. 1).

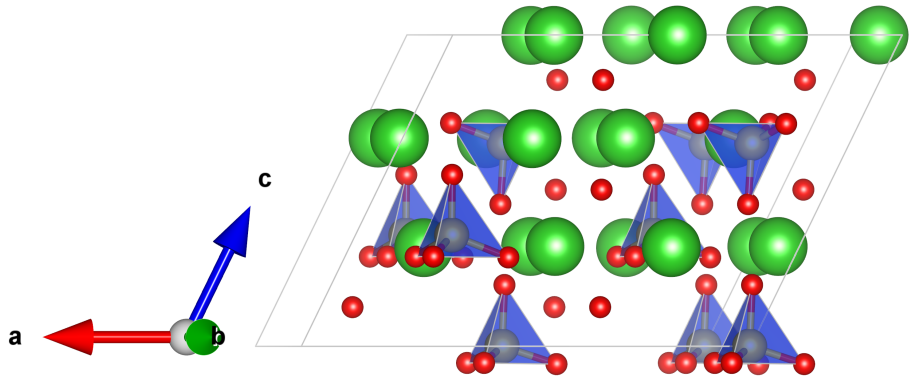

Figure 1: Representation of the C_3S M_3 unit cell. Parameters: a = 12.235 Å, b = 7.073 Å, c = 9.298 Å, β = 116.31°. Color code: calcium cations in green, oxygen anions and silicate oxygen in red, silicon atoms in yellow, and silicate polyhedra in blue.

Because of the Cm space group of the selected model, the only symmetric plane is (010), for which Tasker type 2 surfaces with no net dipole can be built without the need for reconstruction [24, 45] . For the other planes, in order to minimize the dipole moment at the surface, the ions of the cleaved layer were equally distributed on both side of the slab. We constructed for each plane, five unified slabs with random distribution of superficial ions. The size of the slabs was at least 5.6 nm thickness and at least 2.4 nm in the periodic directions, with a 20 nm vacuum between periodic images. The cleaved systems were created by separating the unified slabs in two part along the z axis by a 10 nm vacuum space. For every cleaved and unified system, a serie of 5 steep temperature gradients (10 ps) from 10000 K to 298 K was applied on the superficial atoms in the NVT ensemble (with a Berendsen thermostat), while the rest of the atoms remained fixed. Such a method has already been used to reach more energetically favorable configurations [26, 46], but has never been described so precisely as follows. To avoid moves between two surfaces during this process, each ion was tethered in the z direction by a 1.0 Kcal.mol^{-1}.Å^{-1} spring force. After energy minimization by conjugate gradient method, the lowest energy final configuration of the whole series is subsequently submitted

to a 200 ps equilibration run and to a 300 ps production run in NVT ensemble at 298 K. For the cleaved system, because the cleaved slabs tend to agglomerate, a spring force of 100 Kcal.mol^{-1}.Å^{-1} has been applied to maintain a distance of 10 nm between each surfaces. This process was repeated for several planes perpendicular to the principal directions. Thereafter, the Ca-rich, (040) plane was chosen for this study of the C_3S/water interface. Therefore, the lower slab of the cleaved system (~ 3 nm thick) was used to create an interface system with an equilibrated water slab of 9 nm. Based on the methodology of previous interface studies of Portlandite [17, 19], the periodic images of mineral and water slabs were separated by a vacuum of approximately 7 nm to avoid any interaction through the periodic boundary and to allow the volume of both slabs to fluctuate perpendicularly to the interface and thus lowering the influence of confinement stresses. Four degrees of hydration were investigated, covering pH from largely greater than 15 for the dry C_3S / water interface, to 11.5 for the most hydrated system. To model pH conditions, we applied the last IFF model for hydrated C_3S [31]. The superficial silicate and oxygen anions of the bottom subslab of the cleaved system were protonated, and the charge neutrality of the system was respected, according to the following chemical reactions:

$$\begin{aligned}
O^{2-} &+ H_2O \rightarrow 2OH^- \\
SiO_4^{4-} &+ H_2O \rightarrow HSiO_4^{3-} + OH^- \\
HSiO_4^{3-} &+ H_2O \rightarrow H_2SiO_4^{2-} + OH^- \\
H_2SiO_4^{2-} &+ H_2O \rightarrow H_3SiO_4^- + OH^-
\end{aligned} \tag{1}$$

In the NVT ensemble at 298 K, an equilibration was performed for 0.5 to 1 ns before starting a production run of 2 ns. For the whole set of simulations, the equations of motion were integrated with a 1 fs timestep using the standard Verlet algorithm time integration of the Verlet algorithm and a Nose-Hoover thermostat, with a damping factor of 0.1 ps respectively. The trajectory was recorded for analysis every 0.1 ps. All the simulations were carried out using the LAMMPS package [47]. The PCFF function expression of the INTERFACE FF (PCFF-IFF) was employed to reproduce interactions of both water and C_3S

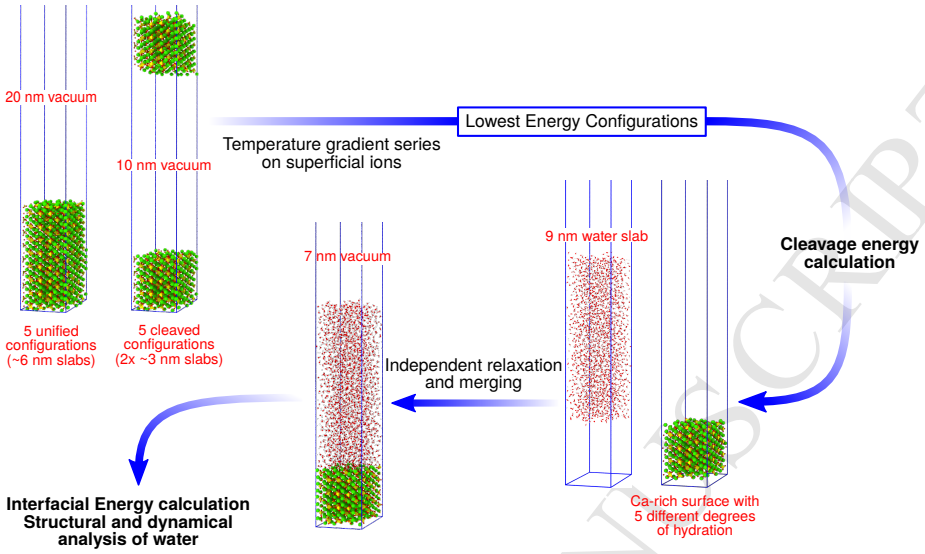

Figure 2: Workflow of the cleavage and interface simulations.

with a cut-off distance of 12 Å for van der Waals interactions and an Ewald summation with an accuracy of 10^{-5} for Coulomb interactions were adopted. The PCFF-IFF potential energy expressed in Eq. (2) contains a 9-6 Lennard-Jones potential with sixth-power mixing rule, and excludes non-bonded interactions for 1-2 and 1-3 bonded atoms:

$$\mathcal{U} = \sum_{ij}\sum_{n=2}^{4} K_{r,ij}(r_{ij} - r_{0,ij})^{\mathrm{n}} + \sum_{ijk}\sum_{n=2}^{4} K_{\theta,ij}(\theta_{ij} - \theta_{0,ij})^{n} + \frac{1}{4\pi\varepsilon_0\varepsilon_r}\sum_{ij}\frac{q_i q_j}{r_{ij}} + \sum_{ij}\varepsilon_{0,ij}\left[2\left(\frac{\sigma_{ij}}{r_{ij}}\right)^{9} - 3\left(\frac{\sigma_{ij}}{r_{ij}}\right)^{6}\right] \quad (2)$$

For water, we employed the full PCFF description of bonded interactions, including cubic and quartic terms of bonded interactions while the PCFF-IFF force field for C_3S only contains quadratic terms. Note that the PCFF-IFF uses partial atomic charges, different from those appearing in the reactions Eq. (1). The whole methodology used in this study is illustrated in Fig. 2.

Miller index	Surface charge density (C/m^2)	Cleavage energy (J/m^2)
(100)	+0.18	1.39 ± 0.03
(300)	-0.09	1.14 ± 0.03
(800)	-0.09	1.17 ± 0.03
(010)	-0.35	1.55 ± 0.04
(040)	+0.35	1.31 ± 0.04
(001)	+0.14	1.38 ± 0.04
(002)	-0.14	1.45 ± 0.04
(003)	+0.14	1.31 ± 0.04
$(00\bar{3})$	+0.14	1.33 ± 0.04
(008)	-0.14	1.22 ± 0.04
$(00\bar{8})$	-0.14	1.22 ± 0.04

Table 1: Cleavage energies for Miller indices in principal directions

3. Results and discussion

3.1. Energy calculation

The cleavage energy is computed from the difference of the averaged energies of the unified and cleaved system, $E_{unified}$ and $E_{cleaved}$, where A is the area of one of the resulting cleaved surfaces (Eq. (3)):

$$E_{cleav} = \frac{E_{cleaved} - E_{unified}}{2A} \tag{3}$$

The cleavage energy values of planes of the principal directions are given in Table 1. The values computed, in the range of 1.14 to 1.55 J/m^2 (1.32 J/m^2 in average) are in good agreement with first results obtained with the same force field, and almost match for the (040) plane (1.31 ± 0.04 J/m^2 against 1324 ± 25 mJ/m^2) [26]. Generally, they are in good agreement with other previous atomistic simulation studies [24, 48]. On the same basis, the interfacial energy is computed by subtracting the energy of the C_3S slab system E_{C_3S} and the energy

System	pH	Interfacial energy (J/m^2)
Dry C_3S	>> 15	-1.42 ± 0.16
1st hyd.	> 15	-1.03 ± 0.17
2nd hyd.	~ 15	-0.64 ± 0.16
3rd hyd.	~ 13.5	-0.60 ± 0.16
4th hyd.	~ 11.5	-0.50 ± 0.16

Table 2: Interfacial energy for different degree of hydration

of the water slab system E_{water} to the energy interface system $E_{C_3S/water}$, and dividing by the contact surface area A:

$$E_{int} = \frac{E_{C_3S/water} - E_{C_3S} - E_{water}}{A} \tag{4}$$

The interfacial energy of simulated systems are given in Table 2 with corresponding pH, according to the last IFF model [31]. The interfacial energy is an indicator of the hydrophilic/hydrophobic behaviour of the surface. The loss of energy in absolute value traduces a more hydrophobic behaviour of the surface as the degree of hydration increases. This behaviour is directly related to the charge distribution occurring during the reactions in Eq. (1), making the hydrogen bonds (H-bonds) between water molecules and surface ions weaker. The energies computed are different and follows the reverse trend than values obtained in previous work [31]. Sign convention and difference in methodology could be the reason for such disagreement. Note that in the present scheme, the water and the C_3S slabs are separated by a vacuum and only interact on one side. The energy of the interface system is greater than the sum of the energies of the two separated systems, because it includes Coulombic and van der Waals interactions between water and C_3S. As expected, the surface is becoming more hydrophobic and hence less reactive upon hydration. The attraction forces between the water molecules and the surface are weakened with hydration of the superficial atomic layer, which is traduced by a decrease in absolute value of the interfacial energy.

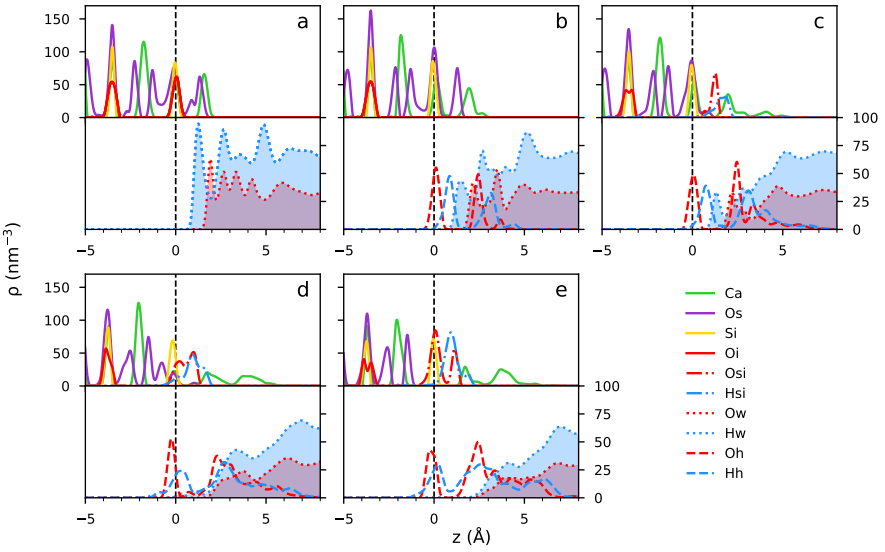

Figure 3: Atomic density profiles of the interface for a) Dry C_3S (pH >> 15), b) 1st hyd. (pH > 15), c) 2nd hyd. (pH ~ 15), d) 3rd hyd. (pH ~ 13.5), e) 4th hyd. (pH ~ 11.5). The interface (z = 0) is defined as the average position of the uppermost layer of silicon atoms. Code for atom nomination: Os for silicate oxygen, Oi for oxygen anion, Oh and Hh for hydroxyl oxygen and hydrogen, Osi and Hsi for silanol oxygen and hydrogen, Ow and Hw for water oxygen and hydrogen.

3.2. Structural properties

The atomic density profile ρ perpendicularly to the surface pictures the structural change occurring with hydration of the first layer of C_3S (Fig. 3).

Looking at the atomic structure of the mineral, the diffusion of calcium cations Ca^{2+} starts slightly with the protonation of oxide O^{2-} to hydroxyl OH^-, but is greatly increased by the first protonation of silicates (SiO_4^{4-} to $HSiO_4^{3-}$). In fact, the structure of C_3S is known to be largely affected by the orientation of silicates, and by the coordination of Ca^{2+} with the oxygen atoms of silicate groups (Os herein) [42]. At pH ~ 11.5, Ca^{2+} and OH^- desorbs up to 4 Å from their initial positions. The partial charges used in this simulation (+1.5 for Ca, and -0.75 for OH^-) allow to describe properly the solid state of C_3S and to balance the charge of the protonation of oxide Oi (with partial charge

-1.5), however the solvated species cannot be reproduced with great accuracy by considering these charges, this is why ionic diffusion in water were not investigated here. Water molecules exhibit a layered organization up to 8 Å from the interface, defined as the average position of the uppermost Si layer. The top Si layer was chosen as reference because its position does not change significantly between each simulation. This behaviour of silicates is consistent with 2 ns reactive MD simulations of C_3S hydration where only rotational motion was observed [24]. The first, strongly bonded water layer is characterized by a clear peak of the Ow atomic density profile at approximately 2.0 Å of the interface with an atomic density of almost twice the bulk atomic density (~ 0.063 $Å^{-3}$). Each water molecule of the first layer share two H-bonds with the oxygen atoms of the surface and three types of hydrogen bonding were identified from the density map: two Hw–Oi bonds (a), two Hw–Os bonds (b), one Hw–Oi and one Hw–Os bond (c) Fig. 4. These three bonding types are the bases of the H-bonds network at the origin of the layered structural arrangement. In the second layer, water molecules form H-bonds with Os or Oi atoms from the surface, and with near water molecules. This intermediate position is more unstable and explains the scattering of the following peaks on the Ow density profile. While the hydration occurs, the strong layered structure formed by water molecules decays with the diffusion of Ca^{2+} and OH^-. After the first protonation reaction (O^{2-} to OH^-), the positions of the three Hw atomic density peaks, and the intensity of the third peak, remain almost unchanged. The decaying of the layered structure becomes much more significant after the protonation of SiO_4^{4-} to $HSiO_4^{3-}$, although the first Ow and Hw atomic density peaks are still observable at pH ~ 15. In the case of the dry surface, every water oxygen atoms are donors, but are becoming progressively acceptors when the protonation state of the surface increases, allowing for Hh–Ow and Hsi–Ow bonds to occur.

The orientation probability distribution (OPD) of a water molecules on the mineral surface gives information on the interactions occurring at the interface. The orientational preference of water molecules within 2.5 Å from the surface is here defined by the angle θ between the z axis, and the dipolar moment of water.

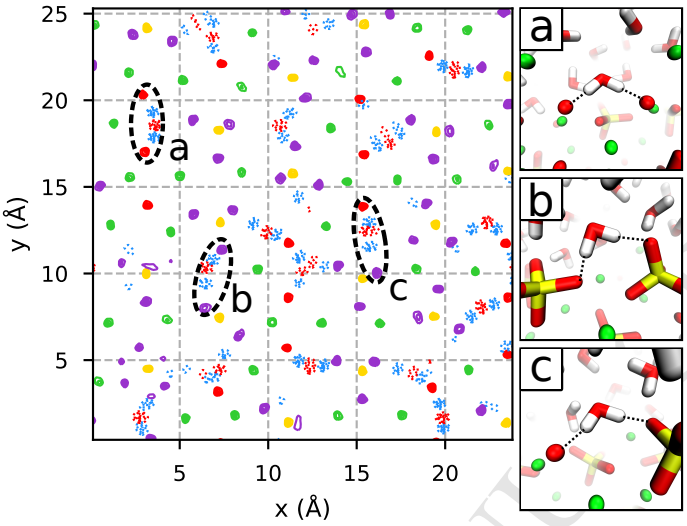

Figure 4: Atomic density maps for dry C_3S / water interface of water molecules of the first layer (0.5 Å < z < 2.4 Å) (left). Zoom on the three hydrogen bonding types: a) two Hw–Oi, b) two Hw–Os bonds, c) one Hw–Oi and one Hw–Os bond (right). Color map: Ca in green, Oi in red, Si in yellow, Os in violet, Ow in red dotted line, Hw in blue dotted line.

Fig. 5 shows the OPD function $P(\theta)$ versus $cos\theta$ for different hydration degree. Water molecules strongly interact with Os and Oi on the C_3S dry surface, which corresponds to a sharp peak at $cos\theta = 1.0$, for the first degree of hydration (pH > 15), a small orientational preference still exists, but $P(\theta)$ can be considered as uniform from the second degree of hydration investigated (first protonation of silicates), traducing a greater rotational motion of water molecules due to a loss of interaction with the surface.

The radial distribution function (RDF), denoted g(r), is a measure of the probability of finding two atoms at a distance r from each other. This parameter is recurrent in MD trajectory analysis, including in other systems [49–52]. Its mathematical expression can be written as follows:

$$g(r) = \lim_{r \to \infty} \frac{p(r)}{4\pi(N/V)r^2 dr} \tag{5}$$

where $p(r)$ is the average number of atom pairs measured at a distance between r and $r + dr$ from each others, N is the number of pairs of atoms, V

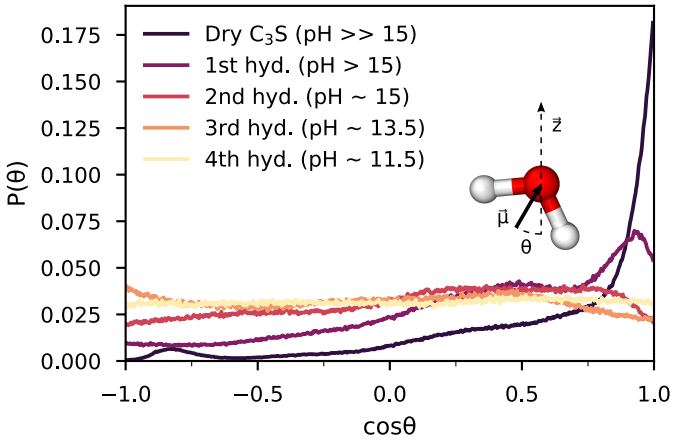

Figure 5: OPD of water molecules within 2.5 Å from the surface with variation of the degree of hydration.

is the total volume of the system. Complementary structural information was given by the RDF between water and C_3S superficial atoms Fig. 6. For Ow-Ow pairs, the RDF was computed between Ow from every water molecules and Ow within 2.5 Å from the surface. The overall observation is that the water atoms lose coordination with the superficial species with increasing of the hydration degree. The coordination peaks of Oi-Hw and Os-Hw are shifted to the right with protonation of Oi and Os to Oh and Osi, traducing a weakening of H-bonds between these species. Oh-Hw pairs have a first coordination shell at ~ 1.7 Å and a second coordination shell at ~ 3.0 Å. Osi-Hw RDF shows a very weak first coordination shell at ~ 1.9 Å, and a second coordination shell at ~ 3.1 Å. Interestingly, a third Osi-Hw coordination shell exists at pH ~ 15 at an inter-atomic distance ~ 6.2 Å. Oh-Hw and Osi-Hw coordination peaks disappear with further hydration. The peak of the first Ca-Ow coordination shell is shifted to the left after the first hydration, due to the start of solvation of Ca^{2+} and the Ca-Ow RDF does not change significantly after the first protonation of silicates. The water interfacial structural features are well represented by the Ow-Ow RDF. A second and third coordination shell peak are present at 5.8 Å and 8.3 Å respectively for water molecules on the dry surface, and decay with

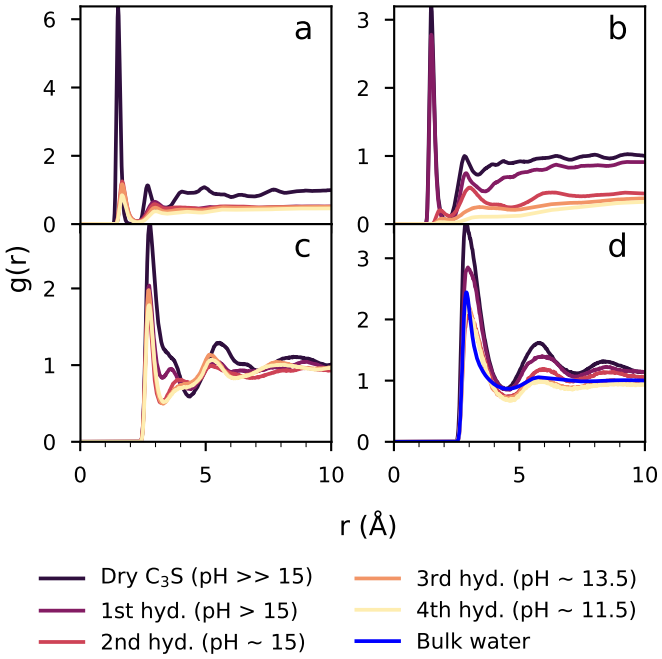

Figure 6: Radial distribution function of a) Oi-Hw and Oh-Hw, b) Os-Hw and Osi-Hw, c) Ca-Ow, d) Ow-Ow, for different degrees of hydration.

hydration of the surface, until matching the Ow-Ow RDF of bulk water.

3.3. Dynamical properties

The investigation of dynamical effects can provide precious information on the interaction between water and mineral surfaces [53]. The dynamical properties of water are significantly altered by the presence of the C_3S surface. In fact, the self-diffusion coefficient (DC) of water molecules decreases importantly from the bulk to the surface. The diffusion coefficient was computed as a function of the mean square displacement (MSD) from the Einstein-Smoluchowski relation:

$$D = \frac{1}{2n} \lim_{t \to \infty} \frac{< [r(t_0 + t) - r(t_0)]^2 >}{\tau} \quad (6)$$

where $< [r(t_0 + t) - r(t_0)]^2 >$ is the double averaged mean square displacement. The first average is applied on the water molecules contained in

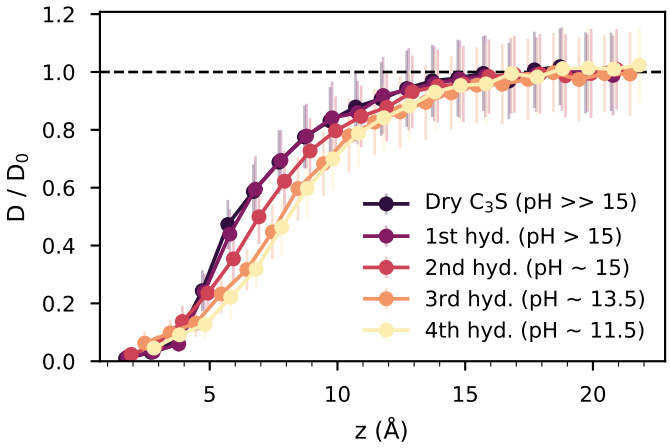

Figure 7: Evolution of the diffusion coefficient of water molecules with distance from the C_3S surface with variation of the degree of hydration. The interface (z = 0) is defined as the average position of the uppermost layer of silica atoms.

the specified group, the second average is performed over time intervals of span τ. Because of the mentioned perturbations caused by the mineral surface, the behaviour of water molecules in an interfacial system is heterogeneous and isotropic. Water molecules are free to desorb and adsorb on the surface, moving along the z axis towards or away from the surface, meaning that depending on the position and the direction considered, the diffusion coefficient will vary. So the observation time τ must be sufficiently long to capture the molecules in diffusive regime, but sufficiently short to represent diffusivity in a specific region. Therefore, based on a calculation method of a previous study [54], the trajectory of the Ow atoms was analyzed updating the selection every 10 ps times slices and in volume slices of 1 Å along the z axis. Within the 10 ps time slice, the DC was computed from the slope of MSD with τ varying from 2 to 8 ps. The evolution with distance from the C_3S surface for different degree of hydration is shown in Fig. 7. Up to 4 Å from the interface, no significant variation has to be noted between simulated systems. For greater distance, the diffusion coefficient D decreases with the degree of hydration of the surface because of the perturbation introduced by the diffusion of Ca^{2+} and OH^- ions. At

approximately 20 Å from the surface, the bulk diffusion coefficient D_0 calculated was ~ 6.25 $\times 10^{-9}$ m^2/s against 7.26 ± 0.02 $\times 10^{-9}$ m^2/s, computed on a cubic box of 30 Å side, at T = 298.0 K in NVT ensemble. This difference could arise from the above described computation method. The shape and the size of the box may also cause such difference [55]. Note that the self-diffusion coefficient of PCFF water is much larger than for flexible SPC water model (3.20 ± 0.03 $\times 10^{-9}$ m^2/s, calculated in the same conditions than for bulk PCFF water), and experimental self-diffusion of pure water (2.3 $\times 10^{-9}$ m^2/s) [56]. Because of differences in structure and dynamics of water models, as well as size and shape effects, the absolute values of DC must be taken with care, and it is purposed here to characterize the decrease in translational mobility of interfacial water molecules with increasing of the degree of hydration of the first atomic layer.

The number of hydrogen bonds that water molecules create with a mineral surface depicts its hydrophilic or hydrophobic behaviour. In this H-bonds analysis, we consider both the number of H-bonds created and their lifetime. The existence of H-bonds was defined by a geometric criterion. For every possible donor, hydrogen, acceptor combination, an H-bonds exists if and only if the distance r between the donor oxygen and the hydrogen is smaller than 2.45 Å, and the angle β between the oxygen donor, the hydrogen and the oxygen acceptor is smaller than 40°. The distance criterion was defined as the first minimum of the O-H radial distribution function of bulk PCFF water. Although an angle of 30° is usually proposed, a larger tolerance was chosen here because of the much larger dispersion in the distribution of β for the PCFF water model compared to the reference SPC model. Even increasing the angle tolerance, the average number of H-bonds at standard state resulted in 3.33 for PCFF bulk against 3.48 for SPC water, and ~3.3 obtained experimentally by K-edge X-ray absorption [57]. The number of H-bonds per water molecule was analyzed along the z axis with variation of the degree of hydration (Fig. 8).

When considering water in contact with the dry C_3S, the total H-bonds number decreases at about 4.7 Å of the first Si layer because of a loss of H-bonds acceptance from water. Ow donates Hw to silicate oxygen Os, and interestingly,

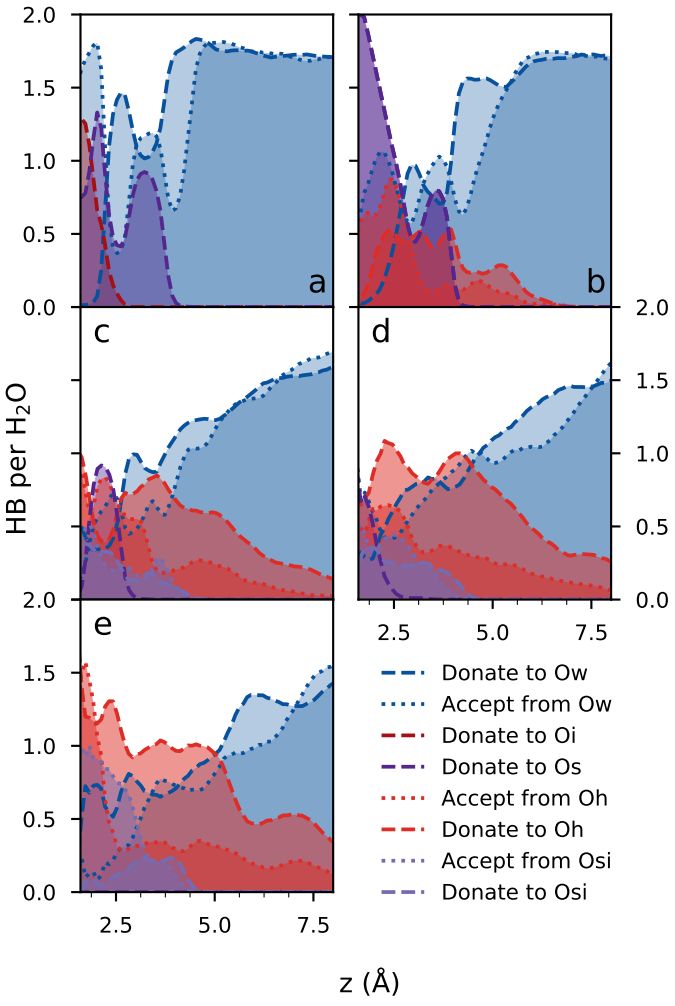

Figure 8: Evolution of the number of hydrogen bonds per water molecules along the z axis with variation of the degree of hydration: a) Dry C_3S (pH >> 15), b) 1st hyd. (pH > 15), c) 2nd hyd. (pH ~ 15), d) 3rd hyd. (pH ~ 13.5), e) 4th hyd. (pH ~ 11.5). The interface (z = 0) is defined as the average position of the uppermost layer of silica atoms.

the water H-bonds acceptance from other water molecules also increases within 2.6 Å to 4.0 Å from the surface. The role of water molecules in this layer (the second layer from the surface) is intermediate between acceptor and donor. They donate on average, approximately one Hw to an Os from the surface and one Hw to an Ow of the first water layer, while they accept one H from the above water molecules. The total H-bonds nearest peak from the surface corresponds to the first water layer observed in the Fig. 3. In this layer, water molecules only donate H-bonds to Oi and Os and accept H-bonds from water molecules of the second layer. For the first hydrated interface (pH >> 15), the hydrogen bonds distribution between water molecules against the distance from the C_3S surface follows the same trend but with a decreased intensity. This is because water molecules are accepting H-bonds from Oh. While the number of Ow-Oi and Ow-Os H-bonds per H_2O was ~1, the preferential interaction site is now Ow-Os due to hydroxylation of Oi and loss of polarity. Hence, the number of Ow-Os H-bonds per H_2O increases near the surface up to 2.0. The distribution of hydrogen bonds between water molecules decays almost linearly from the bulk the surface after the second protonation reaction of silicates (pH < 13.5). As expected with the raising of degree of hydration, water molecules are forming more H-bonds with Osi and Oh (donor and acceptor), and less with Os. The total H-bonds/H_2O is increasing up to 4.6 within 2.5 Å from the most hydrated surface (pH < 11.5) and no H-bond between Ow and Os is reported for this system because the remaining Os atoms point towards the bulk of C_3S. From the protonation of SiO_4^{4-} to $HSiO_4^{3-}$, the hydrogen bonds formed between water molecules is decreasing and water in contact with the surface does not present structural features anymore.

Hydrogen bonds lifetime was measured using the continuous autocorrelation function definition implemented by Gowers and Carbone in the MDAnalysis Python package[58, 59]:

$$C_c(t) = \left\langle \frac{\sum_{i,j} h_{ij}(t_0) h_{ij}(t_0 + t)}{h_{ij}(t_0)^2} \right\rangle \tag{7}$$

τ (ps)	Ow-Oi	Ow-Os	Ow-Oh	Oh-Ow	Ow-Osi	Osi-Ow	Ow-Ow
Dry C_3S	902.79	186.87	—	—	—	—	0.61
1st hyd.	—	146.29	5.19	0.44	—	—	0.37
2nd hyd.	—	14.50	4.87	0.43	1.48	0.90	0.64
3rd hyd.	—	0.96	2.90	0.59	0.31	1.96	0.52
4th hyd.	—	—	2.94	0.08	0.77	1.51	0.49

Table 3: Lifetime of hydrogen bonds with variation of the degree of hydration.

where the binary function $h_{ij}(t)$ is equal to 1 if an H-bonds exists between an acceptor i and a donor j, and 0 if not. In the continuous autocorrelation function, if an H-bonds is broken at a particular moment, it remains broken for the rest of the analysis time and cannot reform. The autocorrelation function $C_c(t)$ is fitted using the sum of two exponential functions and integrating over time:

$$C_c(t) \approx A_1 exp\left(\frac{-t}{\tau_1}\right) + (1 - A_1) exp\left(\frac{-t}{\tau_2}\right) \tag{8}$$

Finally the lifetime τ of the bond is assessed by integrating the fitted function:

$$\tau = \int_0^\infty C_c(t) \tag{9}$$

All the binary function were evaluated every 0.1 ps during the entire production run of 2 ns. The resulting $C_c(t)$ and τ are presented in Table 3. As expected, for the dry C_3S/water interface, the lifetime of Ow-Oi H-bonds is much higher than for Ow-Os. These values are related to the greater acidity of hydroxide anions compared with free silicic acid in water. One should note that in this classical MD study, reactions of dissociation and protonation cannot occur so these two values are overestimated. In fact, water molecules would react preferentially with Oi. On average, and as expected, H-bonds lifetimes are decreasing with decreasing pH.

4. Conclusion

The model used here allowed to assess for the first time the behavior of water molecules on the Ca-rich (040) cleavage plane of M_3 C_3S, with variation of the degree of hydration of the first superficial atomic layer. The layered structure of water, observed at the interface with the surface, decays from the hydration of oxides and is strongly affected by the protonation of silicates SiO_4^{4-} to $HSiO_4^{3-}$. We thus showed that the structural behavior of water is based on the strength of the hydrogen bonds created between the first water layer and the ionic species of the mineral surface. When those hydrogen bonds are stable, the existing network remains well defined and structured. The protonation of oxides and oxygen atoms of silicate leads to changes in charge distribution and weakens hydrogen bonds between the surface and the first water layer. This behavior is reflected in the orientation probability distribution water molecules of the first layer. A preferential orientation of water molecules on the dry C_3S exists because of the three bonding types observed (namely Oi-Ow-Oi, Os-Ow-Os and Oi-Ow-Os), whereas H_2O molecules gain rotational motion when hydration occurs, with uniform orientation probability distribution. In the range of 4 Å to 16 Å from the interface, their translational motion decreases with the degree of hydration because of the perturbation introduced by the solvated ionic species. The study of dynamical properties such as diffusion and lifetime hydrogen bonds adds new insights into the interfacial behavior related to hydration reactions. An even better accuracy regarding dissociation and solvation can be obtained by changing the charge of calcium cations and/or modifying the water model [26]. The present simulations treat the protonation steps incrementally, and allowed to describe the behavior of water at several degree of hydration of the first atomic layer. Reactive MD as well as *ab initio* MD are appropriate methods to investigate water dissociation and protonation reactions towards a better understanding of mechanisms responsible for dissolution and formation of C-S-H. This study is in progress. As another proposal for future investigation, the influence of impurities on C_3S hydration might also be taken into account.

Acknowledgements

The authors acknowledge Brazilian science agencies CAPES (PDSE process n°88881.188619/2018-01) and CNPq for financial support, as well as Andrey Kalinichev and Hendrik Heinz for helpful discussions.

References

[1] R. M. Andrew, Global CO_2 emissions from cement production, Earth System Science Data 10 (1) (2018) 195–217. doi:10.5194/essd-10-195-2018.

[2] K. L. Scrivener, P. Juilland, P. J. Monteiro, Advances in understanding hydration of Portland cement, Cement and Concrete Research 78 (2015) 38–56. doi:10.1016/j.cemconres.2015.05.025.

[3] E. Gartner, Discussion of the paper "Dissolution theory applied to the induction period in alite hydration" by P. Juilland et al., cem. concr. res. 40 (2010) 831-844, Cement and Concrete Research 41 (5) (2011) 560–562. doi:10.1016/j.cemconres.2011.01.019.

[4] P. Juilland, E. Gallucci, R. Flatt, K. Scrivener, Dissolution theory applied to the induction period in alite hydration, Cement and Concrete Research 40 (6) (2010) 831–844. doi:10.1016/j.cemconres.2010.01.012.

[5] H. F. W. Taylor, P. Barret, P. W. Brown, D. D. Double, G. Frohnsdorff, V. Johansen, D. Ménétrier-Sorrentino, I. Odler, L. J. Parrott, J. M. Pommersheim, M. Regourd, J. F. Young, The hydration of tricalcium silicate, Materials and Structures 17 (6) (1984) 457–468. doi:10.1007/bf02473986.

[6] J. S. Dolado, M. Griebel, J. Hamaekers, A molecular dynamic study of cementitious calcium silicate hydrate (C-S-H) gels, Journal of the American Ceramic Society 90 (12) (2007) 3938–3942. doi:10.1111/j.1551-2916.2007.01984.x.

[7] H. Manzano, S. Moeini, F. Marinelli, A. C. T. van Duin, F.-J. Ulm, R. J.-M. Pellenq, Confined water dissociation in microporous defective silicates: Mechanism, dipole distribution, and impact on substrate properties, Journal of the American Chemical Society 134 (4) (2012) 2208–2215. doi:10.1021/ja209152n.

[8] R. J.-M. Pellenq, A. Kushima, R. Shahsavari, K. J. V. Vliet, M. J. Buehler, S. Yip, F.-J. Ulm, A realistic molecular model of cement hydrates, Proceedings of the National Academy of Sciences 106 (38) (2009) 16102–16107. doi:10.1073/pnas.0902180106.

[9] P. A. Bhat, N. Debnath, Theoretical and experimental study of structures and properties of cement paste: The nanostructural aspects of C-S-H, Journal of Physics and Chemistry of Solids 72 (8) (2011) 920–933. doi:10.1016/j.jpcs.2011.05.001.

[10] M. J. A. Qomi, M. Bauchy, F.-J. Ulm, R. J.-M. Pellenq, Anomalous composition-dependent dynamics of nanoconfined water in the interlayer of disordered calcium-silicates, The Journal of Chemical Physics 140 (5) (2014) 054515. doi:10.1063/1.4864118.

[11] M. Bauchy, M. J. A. Qomi, F.-J. Ulm, R. J.-M. Pellenq, Order and disorder in calcium–silicate–hydrate, The Journal of Chemical Physics 140 (21) (2014) 214503. doi:10.1063/1.4878656.

[12] A. Lushnikova, A. Zaoui, Improving mechanical properties of C-S-H from inserted carbon nanotubes, Journal of Physics and Chemistry of Solids 105 (2017) 72–80. doi:10.1016/j.jpcs.2017.02.010.

[13] J. Fu, F. Bernard, S. Kamali-Bernard, Assessment of the elastic properties of amorphous calcium silicates hydrates (i) and (II) structures by molecular dynamics simulation, Molecular Simulation 39 (2017) 1–15. doi:10.1080/08927022.2017.1373191.

[14] J. Yang, D. Hou, Q. Ding, Ionic hydration structure, dynamics and adsorption mechanism of sulfate and sodium ions in the surface of calcium silicate hydrate gel: A molecular dynamics study, Applied Surface Science 448 (2018) 559–570. doi:10.1016/j.apsusc.2018.04.071.

[15] S. M. Mutisya, J. M. de Almeida, C. R. Miranda, Molecular simulations of cement based materials: A comparison between first principles and classical force field calculations, Computational Materials Science 138 (2017) 392–402. doi:10.1016/j.commatsci.2017.07.009.

[16] S. M. Mutisya, C. R. Miranda, The surface stability and morphology of tobermorite 11 Å from first principles, Applied Surface Science 444 (2018) 287–292. doi:10.1016/j.apsusc.2018.03.002.

[17] S. Galmarini, A. Aimable, N. Ruffray, P. Bowen, Changes in portlandite morphology with solvent composition: Atomistic simulations and experiment, Cement and Concrete Research 41 (12) (2011) 1330–1338. doi:10.1016/j.cemconres.2011.04.009.

[18] S. Galmarini, A. K. Mohamed, P. Bowen, Atomistic simulations of silicate species interaction with portlandite surfaces, The Journal of Physical Chemistry C 120 (39) (2016) 22407–22413. doi:10.1021/acs.jpcc.6b07044.

[19] S. Galmarini, P. Bowen, Atomistic simulation of the adsorption of calcium and hydroxyl ions onto portlandite surfaces — towards crystal growth mechanisms, Cement and Concrete Research 81 (2016) 16–23. doi:10.1016/j.cemconres.2015.11.008.

[20] H. Manzano, R. J. M. Pellenq, F.-J. Ulm, M. J. Buehler, A. C. T. van Duin, Hydration of Calcium Oxide Surface Predicted by Reactive Force Field Molecular Dynamics, Langmuir 28 (9) (2012) 4187–4197. doi:10.1021/la204338m.

[21] J. Fu, F. Bernard, S. Kamali-Bernard, First-principles calculations of typical anisotropic cubic and hexagonal structures and homogenized moduli estimation based on the y-parameter: Application to CaO, MgO, CH and calcite CaCO3, Journal of Physics and Chemistry of Solids 101 (2017) 74–89. doi:10.1016/j.jpcs.2016.10.010.

[22] R. Shahsavari, L. Chen, Screw dislocations in complex, low symmetry oxides: Core structures, energetics, and impact on crystal growth, ACS Applied Materials & Interfaces 7 (4) (2015) 2223–2234. doi:10.1021/am5091808.

[23] R. Shahsavari, L. Tao, L. Chen, Structure, energetics, and impact of screw dislocations in tricalcium silicates, Journal of the American Ceramic Society 99 (7) (2016) 2512–2520. doi:10.1111/jace.14255.

[24] H. Manzano, E. Durgun, I. López-Arbeloa, J. C. Grossman, Insight on Tricalcium Silicate Hydration and Dissolution Mechanism from Molecular Simulations, ACS Applied Materials & Interfaces 7 (27) (2015) 14726–14733. doi:10.1021/acsami.5b02505.

[25] Q. Wang, H. Manzano, Y. Guo, I. Lopez-Arbeloa, X. Shen, Hydration Mechanism of Reactive and Passive Dicalcium Silicate Polymorphs from Molecular Simulations, The Journal of Physical Chemistry C 119 (34) (2015) 19869–19875. doi:10.1021/acs.jpcc.5b05257.

[26] R. K. Mishra, R. J. Flatt, H. Heinz, Force Field for Tricalcium Silicate and Insight into Nanoscale Properties: Cleavage, Initial Hydration, and Adsorption of Organic Molecules, The Journal of Physical Chemistry C 117 (20) (2013) 10417–10432. doi:10.1021/jp312815g.

[27] Y. Zhang, X. Lu, Z. He, D. Song, Molecular and dissociative adsorption of a single water molecule on a β-dicalcium silicate (100) surface explored by a DFT approach, Journal of the American Ceramic Society 101 (6) (2017) 2428–2437. doi:10.1111/jace.15381.

[28] H. Zhao, Y. Wang, Y. Yang, X. Shu, H. Yan, Q. Ran, Effect of hydrophobic groups on the adsorption conformation of modified polycarboxylate superplasticizer investigated by molecular dynamics simulation, Applied Surface Science 407 (2017) 8–15. doi:10.1016/j.apsusc.2017.02.132.

[29] D. Tavakoli, A. Tarighat, Molecular dynamics study on the mechanical properties of portland cement clinker phases, Computational Materials Science 119 (2016) 65–73. doi:10.1016/j.commatsci.2016.03.043.

[30] R. K. Mishra, A. K. Mohamed, D. Geissbühler, H. Manzano, T. Jamil, R. Shahsavari, A. G. Kalinichev, S. Galmarini, L. Tao, H. Heinz, R. Pellenq, A. C. van Duin, S. C. Parker, R. J. Flatt, P. Bowen, cemff : A force field database for cementitious materials including validations, applications and opportunities, Cement and Concrete Research 102 (2017) 68–89. doi:10.1016/j.cemconres.2017.09.003.

[31] E. Pustovgar, R. K. Mishra, M. Palacios, J.-B. d'Espinose de Lacaillerie, T. Matschei, A. S. Andreev, H. Heinz, R. Verel, R. J. Flatt, Influence of aluminates on the hydration kinetics of tricalcium silicate, Cement and Concrete Research 100 (2017) 245–262. doi:10.1016/j.cemconres.2017.06.006.

[32] H. Heinz, T.-J. Lin, R. K. Mishra, F. S. Emami, Thermodynamically consistent force fields for the assembly of inorganic, organic, and biological nanostructures: The INTERFACE force field, Langmuir 29 (6) (2013) 1754–1765. doi:10.1021/la3038846.

[33] R. T. Cygan, J.-J. Liang, A. G. Kalinichev, Molecular models of hydroxide, oxyhydroxide, and clay phases and the development of a general force field, The Journal of Physical Chemistry B 108 (4) (2004) 1255–1266. doi:10.1021/jp0363287.

[34] A. C. T. van Duin, S. Dasgupta, F. Lorant, W. A. Goddard, ReaxFF: A Reactive Force Field for Hydrocarbons, The Journal of Physical Chemistry A 105 (41) (2001) 9396–9409. doi:10.1021/jp004368u.

[35] T. P. Senftle, S. Hong, M. M. Islam, S. B. Kylasa, Y. Zheng, Y. K. Shin, C. Junkermeier, R. Engel-Herbert, M. J. Janik, H. M. Aktulga, T. Verstraelen, A. Grama, A. C. T. van Duin, The ReaxFF reactive force-field: development, applications and future directions, npj Computational Materials 2 (1). doi:10.1038/npjcompumats.2015.11.

[36] H. Heinz, U. W. Suter, Atomic charges for classical simulations of polar systems, The Journal of Physical Chemistry B 108 (47) (2004) 18341–18352. doi:10.1021/jp048142t.

[37] L. Wang, D. Hou, H. Shang, T. Zhao, Molecular dynamics study on the tricalcium silicate hydration in sodium sulfate solution: Interface structure, dynamics and dissolution mechanism, Construction and Building Materials 170 (2018) 402–417. doi:10.1016/j.conbuildmat.2018.03.035.

[38] K. L. Scrivener, A. Nonat, Hydration of cementitious materials, present and future, Cement and Concrete Research 41 (7) (2011) 651–665. doi:10.1016/j.cemconres.2011.03.026.

[39] A. G. Kalinichev, J. Wang, R. J. Kirkpatrick, Molecular dynamics modeling of the structure, dynamics and energetics of mineral–water interfaces: Application to cement materials, Cement and Concrete Research 37 (3) (2007) 337–347. doi:10.1016/j.cemconres.2006.07.004.

[40] A. Alex, A. K. Nagesh, P. Ghosh, Surface dissimilarity affects critical distance of influence for confined water, RSC Adv. 7 (6) (2017) 3573–3584. doi:10.1039/c6ra25758e.

[41] T. Q. Vo, B. Kim, Transport phenomena of water in molecular fluidic channels, Scientific Reports 6 (1). doi:10.1038/srep33881.

[42] H. F. W. Taylor, Cement Chemistry, Academic Pr, 1990.

[43] W. Mumme, Crystal structure of tricalcium silicate from a portland cement clinker and its application to quantitative xrd analysis, Neues Jahrbuch fuer Mineralogie: Monatshefte 4 (1995) 145–160.

[44] H. Manzano, E. Durgun, M. J. A. Qomi, F.-J. Ulm, R. J. M. Pellenq, J. C. Grossman, Impact of chemical impurities on the crystalline cement clinker phases determined by atomistic simulations, Crystal Growth & Design 11 (7) (2011) 2964–2972. doi:10.1021/cg200212c.

[45] P. W. Tasker, The stability of ionic crystal surfaces, Journal of Physics C: Solid State Physics 12 (22) (1979) 4977–4984. doi:10.1088/0022-3719/12/22/036.

[46] Y.-T. Fu, H. Heinz, Cleavage energy of alkylammonium-modified montmorillonite and relation to exfoliation in nanocomposites: Influence of cation density, head group structure, and chain length, Chemistry of Materials 22 (4) (2010) 1595–1605. doi:10.1021/cm902784r.

[47] S. Plimpton, Fast parallel algorithms for short-range molecular dynamics, Journal of Computational Physics 117 (1) (1995) 1–19. doi:10.1006/jcph.1995.1039.

[48] E. Durgun, H. Manzano, P. V. Kumar, J. C. Grossman, The Characterization, Stability, and Reactivity of Synthetic Calcium Silicate Surfaces from First Principles, The Journal of Physical Chemistry C 118 (28) (2014) 15214–15219. doi:10.1021/jp408325f.

[49] G. G. Almeida, A. Borges, J. M. Cordeiro, On the hydrogen bonding between n-methylformamide and acetone and tetrahydrofuran, Chemical Physics 434 (2014) 25–29. doi:10.1016/j.chemphys.2014.02.013.

[50] G. G. Almeida, J. M. M. Cordeiro, M. E. Martín, M. A. Aguilar, Conformational changes of the alanine dipeptide in water–ethanol binary mixtures, Journal of Chemical Theory and Computation 12 (4) (2016) 1514–1524. doi:10.1021/acs.jctc.5b00952.

[51] J. M. M. Cordeiro, A. K. Soper, A hybrid neutron diffraction and computer simulation study on the solvation of n-methylformamide in dimethyl-

sulfoxide, The Journal of Chemical Physics 138 (4) (2013) 044502. doi:10.1063/1.4773346.

[52] J. M. Cordeiro, A. K. Soper, Investigation on the structure of liquid n-methylformamide–dimethylsulfoxide mixtures, Chemical Physics 381 (1-3) (2011) 21–28. doi:10.1016/j.chemphys.2011.01.003.

[53] R. J. Kirkpatrick, A. G. Kalinichev, J. Wang, Molecular dynamics modelling of hydrated mineral interlayers and surfaces: structure and dynamics, Mineralogical Magazine 69 (3) (2005) 289–308. doi:10.1180/0026461056930251.

[54] I. C. Bourg, C. I. Steefel, Molecular dynamics simulations of water structure and diffusion in silica nanopores, The Journal of Physical Chemistry C 116 (21) (2012) 11556–11564. doi:10.1021/jp301299a.

[55] G. Kikugawa, S. Ando, J. Suzuki, Y. Naruke, T. Nakano, T. Ohara, Effect of the computational domain size and shape on the self-diffusion coefficient in a lennard-jones liquid, The Journal of Chemical Physics 142 (2) (2015) 024503. doi:10.1063/1.4905545.

[56] K. Krynicki, C. D. Green, D. W. Sawyer, Pressure and temperature dependence of self-diffusion in water, Faraday Discussions of the Chemical Society 66 (1978) 199. doi:10.1039/dc9786600199.

[57] J. D. Smith, Energetics of hydrogen bond network rearrangements in liquid water, Science 306 (5697) (2004) 851–853. doi:10.1126/science.1102560.

[58] R. J. Gowers, P. Carbone, A multiscale approach to model hydrogen bonding: The case of polyamide, The Journal of Chemical Physics 142 (22) (2015) 224907. doi:10.1063/1.4922445.

[59] N. Michaud-Agrawal, E. J. Denning, T. B. Woolf, O. Beckstein, MDAnalysis: A toolkit for the analysis of molecular dynamics simulations,

Journal of Computational Chemistry 32 (10) (2011) 2319–2327. doi:10.1002/jcc.21787.

HIGHLIGHTS

- Molecular Dynamics simulation is used to investigate the water behaviour at interface with Tricalcium Silicate
- Hydrogen bonds network in interfacial water is weaken by the protonation of superficial oxides and silicates
- Translational motion of interfacial water decrease with the degree of hydration
- Water molecules in contact with the dry C_3S have dipole moments pointing preferentially away from the surface.
- Rotational motion of interfacial water increase with the degree of hydration